Wasit Journal of Engineering Sciences
Journal homepage: https://ejuow.uowasit.edu.iq
Vol. 14 No. 2 June 2026, pp.504-521
https://doi.org/10.31185/ejuow.v14i2.939

ISSN 2305-6932
Original Research

Green Synthesis and Characterization of Fe_3O_4@SiO_2@$AgVO_3$ Magnetic Composites for Efficient Removal of Methylene Blue from Aqueous Solution

Alaa Waleed Juma1, Nuralhuda Aladdin Jasim2, Alaa Kharbat Shadhar3, Wisam Fawzi4
[1] Environmental and water Engineering Department, College of Engineering, Wasit University, Iraq
[2, 3] Civil Engineering Department, College of Engineering, Wasit University, Iraq
[4]Civil Engineering Department, Engineering Faculty, Babol Noshirvani University of Technology (NIT), Mazendaran, Iran

Corresponding Author Email: njasim@uowasit.edu.iq

Received Apr.12, 2026 Revised May.21, 2026 Accepted May.31, 2026 Online Jun.1, 2026

ABSTRACT

The application of synthetic dyes has grown as a result of the development of the textile industry in Iraq, which has resulted in detrimental effects on the environment in terms of their inability to decompose naturally. The magnetic composites Fe_3O_4@SiO_2@$AgVO_3$, which are coated with silica and silver vanadate, were produced using an environmentally friendly method. Afterwards, synthetic dyes like methylene blue (MB) were extracted from aqueous solutions using these composites. An alternative to the more conventional method may be implemented as a green synthesis method to produce green nanomaterials that are highly sustainable and recoverable via magnet. Composites in the core-shell structure were 89 % efficient in removal, and in the supported structure, the composites were found to be 91% efficient. Helped system efficiency was a little bit greater because of the availability of active areas. The characterization process confirmed the productive synthesis and strong magnetism and, along with it, easy separation and production to recycle. The atomic force microscopy (AFM) and transmission electron microscopy (TEM) revealed that the iron core had a constant shape and had been sufficiently covered in silica as well as $AgVO_3$. Particularly, the conclusions indicate that Fe_3O_4/SiO_2/$AgVO_3$ can be used sustainably to remove the toxic synthetic dyes like Methylene Blue in the wastewater and other environmental cleanup programs.

Keywords: Green synthesis, TEM, AFM, MB, core/shell, supported, nanocomposite, catalysts.

1. Introduction

Water forms a crucial component of the universe as all living objects in the world depend on it to live. There are many natural and man-made sources of water on Earth, such as glaciers, mountains, oceans, rivers, lakes, and aquariums [1]. The hydrological cycle is a process by which water is moved across the resources of the universe and it involves precipitation, evaporation, freezing, melting and condensation [2]. There is water covering almost 71% of the planet. In contrast to the land, this makes up 2.5 percent of all the water on the planet, oceans hold 97.5 percent [3, 4]. The ice caps and glaciers supply one and a half percent of all fresh water in the world, but the ninety-eight and a half percent is supplied by other sources. Just less than 90% of the world's fresh water is located underground, as groundwater.

The remaining 10 percent is found in the soil, water vapor in the atmosphere and surface water bodies including rivers, dams, lakes and ponds [5]. Most parts of the world have limited supplies of portable water. The major causes of water shortage are the soaring population of the global population, the devastation of natural sources of water by human beings, the advent of industrialization and the pollution of the water sources by the massive urbanization [6]. Water pollution can be defined as the contaminants of water bodies

which have reached levels that render it to be unfit to be used by humans to drink, cook, bathe and other uses. Water pollution is a type of water contamination where some elements or conditions are contained in water in a form that limits the utility of the water in a specific application [7]. Water rivulets might be polluted with a large number of contaminating substances. Out of the aquatic ecosystems in Europe, 572 new pollutants have been identified [8]. When the pollutants are disposed of in the environment, this is known as pollution [9]. The total estimated amount of municipal wastewater generated in a year is 380 billion m 3 and the rate of its rise was estimated to be 24 percent in 2030 and 51 percent in 2050 according to the European Investment Bank [10]. The major sources of water pollution are businesses, homes, and farms. The industries release different toxins into the water bodies yearly in the form of toxic sludge, heavy metals, and solvents among others. Eighty percent of the industrial wastewater treatment plans in the world are wastewater treatment plants. Water pollution is also a major factor that is caused by agriculture because of the huge volumes of water used by the agricultural industry [11]. Additionally, the discharge of several harmful pollutants to water bodies, including microplastics, radionuclides, oil, pharmaceuticals, dyes, pesticides and compounds containing phosphorus and nitrogen, adversely affects the lives of both land and water-dwelling organisms [12, 13].
These pollutants are inconceivably toxic, cancer causing, bio-refractory and bio-accumulative at very small concentrations.
One of the most common types of pollutants found in water bodies is organic contaminants. A large repertoire of organic pollutants have been discovered to be mutagenic, or carcinogenic and hence generally harmful to human health and other ecological systems. This evidence points out the dire need to study and develop a dependable way of removing these contaminants out of water [14]. The main form of biological waste is dye pollution that is mostly discharged into water by industries. Colorants in many different businesses are dyed, including food, textile and pharmaceutical. These colors pose a great risk to the health of the human and natural environment since they leak into the water bodies [15]. Dyeing can be defined as the act of coloring one material with the help of some chemical substances. Dyes may be applied to hair, fur, wax, paper, leather, fiber, cosmetic base and even food [16]. Over 100,000 commercially available dyes are produced each year and consist of about 7×10^1 tons of dyestuff. There is no secret that heavy metals and dyes to a great extent cause the perception of people regarding the quality of water to change and raises the question of environmental pollution and health hazard of people using the contaminated water resources. Dyes are produced by industries in paper, textiles, leather, rubber, plastic and printing [17]. In the dying process, ten to fifteen percent of all the dye made in the world is released as effluents in the textile industry [18]. The 12 percent of synthetic dyes are lost in the process of making the dusties. These include: methyl red, methylene blue, rhodamine b, Remazol Brilliant Blue, and Congo red among others [19]. A significant threat to aquatic systems is the use of dyes and pigments because they require a high amount of oxygen (both chemical and biological) (150 30,000 and 80 6,000 mg/L) [20]. The Direct Black 38 [21] has been associated with cancer bladder and urinary tract cancer. Similarly, the Direct Blue 15 causes mutations [22].
The hazards of anthraquinone dyes are similar. The Val Green 3 (VG3) is very toxic to algae and daphnids; at 0.5 mg/L, it causes death to algae [23].One example of a contaminant that has an impact on both land and water life is methylene blue (MB). Thirdly, we should devise more efficient and effective ways of filtering these contaminants in drinking water [24]. Photocatalysis is one of the technologies which are becoming increasingly popular as it is rapid, effective, cheap and less harmful to the environment [25]. The contaminants are dissolvable in the wastewater in an energy-free process that uses the energy produced by sunlight [26], [27].
Industrial dye effluents are known as the main source of water pollution mainly due to the persistence, toxicity and bright color intensity of synthetic dyes especially from textile industry [28]. These dyes can negatively impact aquatic ecosystems by rapid decreases in photosynthetic activity and biological processes and might also increase risks to human health. These dyes are difficult to remove from wastewater using traditional methods, thus highlighting the need for effective and sustainable treatment technologies [29].
Given the green and mild methodology of photocatalytic degradation with mineralization ability for contaminants, this novel approach has become a promising method to remove dyes. Due to its chemical stability, it is a strong chromophore that can be easily monitored and has been well characterized in both photocatalytic and adsorption studies [22]. Methylene Blue (MB) was chosen as the model dye contaminant. While MB is not one of the major industrial dyes in textiles, its use enables standardization for evaluating photocatalytic performance.
Although photocatalytic studies have advanced over the past decade, there remains an outstanding need for research and development to optimise photocatalyst efficiency as well as a potential research gap in relation to the cost-effective & environmentally benign materials. This study describes the evaluation of two types of

catalysts for photocatalytic degradation of MB and significance, [e.g., due to the novel synthesis method, combination with different materials or comparison with other operational conditions]. This study called for to advance useful solutions to synthetic dye contamination in the water network.

As a model dye contaminant, Methylene Blue (MB) was selected because of its chemical stability, dark blue color for easy monitoring, and well-established behavior in both photocatalytic and adsorption studies. However, since MB is not one of the high-volume industrial textile dyes, its use provides a uniform test permitting evaluation of photocatalytic performance under well controlled experimental conditions.

This paper aims to summarize and describe two kinds of $Fe_3O_4@SiO_2@AgVO_3$ magnetic composites, i.e., core/shell and supported nanocomposites, using a green synthesis process. Their ability to extract methylene blue (MB) in aqueous solutions will be established in the paper. The paper will analyze the suitability of the two kinds of composites as sustainable and effective wastewater treatment materials by studying their structural, magnetic, and photocatalytic properties and their effectiveness in the treatment of organic dye contaminants, such as methylene blue.

2. Substances and techniques

2.1. Components

All compounds were used in their exact quantitative forms and underwent no further purification. The following resources were utilized for this investigation: Histidine, or ferric chloride,•6(H_2O)(97%), ferrous sulfate heptahydrate ($FeSO_4$), sourced from Thomas Baker in India Ingredients: •7H_2O (99%, Alpha Chemika, India), tetraethyl orthosilicate $Si(OC_2H_5)_4$ (98%, Sigma-Aldrich, China), sodium hydroxide (NaOH, 99.88%, SDFCL), ethanol (C_2H_5OH, 100%, Thomas Baker), ammonia solution (NH_4OH, 25%, Thomas Baker, India), hydrogen peroxide (H_2O_2, 35%, Panreac, China), hydrochloric acid (HCl, 35-38%, Thomas Baker), and methylene blue $C_{16}H_{18}ClN_3S$ (excellent, HiMedia). The properties of the experimental materials are shown in Table 1.

Table 1. The characteristics of the laboratory reagents used in the experimental method.

Chemicals	Chemical name	Purities	Manufacturer	Mol. Wt.
Ferric chloride hexahydrate	$FeCl_3·6H_2O$	97%	Thomas Baker, India	270.3
Ferrous sulfate heptahydrate	$FeSO_4·7H_2O$	99%	Alpha Chemika, India	278.0
Tetraethyl orthosilicate (TEOS)	$Si(OC_2H_5)_4$	98%	Sigma-Aldrich, China	208.3
Sodium hydroxide	NaOH	99.88%	SDFCL	40.0
Ethanol	C_2H_5OH	100%	Thomas Baker	46.07
Ammonia solution	NH_4OH	25%	Thomas Baker, India	35.05
Hydrogen peroxide	H_2O_2	35%	Panreac, China	34.01
Hydrochloric acid	HCl	35-38%	Thomas Baker	36.46
Methylene blue	$C_{16}H_{18}ClN_3S$	Pure	HiMedia	319.85
Silver nitrates	$AgNO_3$	99.8%	ODAEJUNG, China	169.87
Ammonium metavanadate	NH_4VO_3	99%	CDH Fine Chemicals India,	116.98

2.2. Preparation of Mandarin Peel Extract

The clean mandarin peels were gathered from nearby vendors, rinsed them, and then sterilized them in a 77% ethanol solution. After a day of air drying, the peels were placed in a hot-air oven set at 60°C for a further 72 hours of drying. 10 g of powdered mandarin peel was carefully weighed on an analytical balance (Ohaus Adventurer) and transferred to an Erlenmeyer flask after being ground in an electric grinder. For the purpose of synthesising Fe_3O_4 NPs, 150 mL of distilled water was added to the flask. The mixture was heated to 40°C for 2 hours while continuously stirred at 500 rpm using a magnetic stirrer. After filtering twice through Whatman No. 1 filter paper, the extract was stored at 4 °C in a tight glass bottle, as shown in Figure 1.

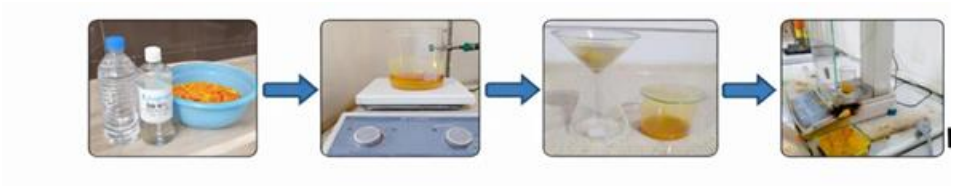

Figure 1. Preparation of Mandarin Peel Extract

2.3. Properties of Fe_3O_4 nanoparticles

The exceptional properties of Fe_3O_4 NPs have made them promising materials in materials research. Fe_3O_4 NPs are incredibly adaptable due to their superb thermal, optical, structural, physical, magnetic, and electrical properties (Table 2). [17].

Table 2. General properties of Fe3O4 (magnetite).

Property	Value
Molecular Formula	Fe_3O_4
Color	Jet black
Melting Point	1583–1597 (°C)
Saturation Magnetization (Ms) at 300 K	92–100 [emu·g^{-1}]
Density	5.18 (g/cm^3)
Type of Magnetism	Ferrimagnetic
Curie Temperature (Tc)	858 (K)
Band Gap Energy (Eg)	2.6 [eV]
Crystallographic System	Cubic
Structure Type	Inverse spinel
Lattice Parameter (nm)	α = b = c = 0.8396
Lattice Angles	α = β = γ = 90°
Standard Gibbs Free Energy of Formation (ΔG^{o}f)	−1012.6 [kJ/mol]

2.4. Synthesis of Fe_3O_4 MNPs.

Magnetic nanoparticles (MNPs) made of Fe_3O_4 were produced by the co-precipitation technique (figure 2). The following molar ratios were maintained: 0.25 mol (0.695 g) of $FeSO_4$•$7H_2O$ and 0.25 mol (1.35 g) of $FeCL_3$•$6H_2O$ were dissolved in 10 mL and 20 mL of deionized water, respectively. After mixing the two solutions in a glass beaker, 50 mL of mandarin peel extract was added. To allow the iron precursors and extract to interact thoroughly, the mixture was agitated continuously for 30 minutes. Stir the mixture for another hour at 80°C after adding NH_4OH (12 M, 30 mL) dropwise until the pH hits 9-10. After centrifugation at 5000 rpm for 10 minutes, the precipitate was collected. It was then washed five times with deionized water and then rinsed with ethanol to eliminate any remaining organic and surface contaminants. Referring to Figure 2, the specimen was subjected to a hot air oven drying process at 80°C for three to six hours before being sealed in an airtight container to avoid loss of moisture.

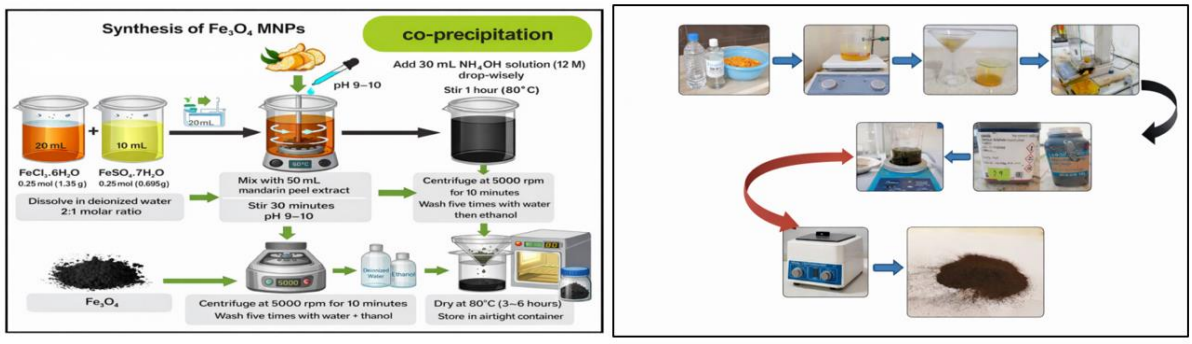

Figure 2. Synthesis of Fe_3O_4 Magnetic Nanoparticles (MNPs) via Co-precipitation.

2.5. Synthesis of Fe_3O_4@SiO_2 MNCs

The following ingredients were used: 10 mL of deionized water, 30 mL of 100% ethanol (CH_3CH_2OH, ≥99.8%; Sigma-Aldrich), and 1 mL of ammonia solution (30% NH_3; Applichem Panreac) with 0.5 g of FeO_4 nanoparticles scattered throughout. Uniform dispersion was achieved by sonication for 30 minutes. Next, 2.5 mL of tetraethyl orthosilicate (TEOS, ≥99.0%; Fluka) was added dropwise while stirring continuously. The mixture was stirred at room temperature for 22 hours. After that, it was washed with ethanol to remove any organic and surface contaminants. Preparation for further studies involved collecting and drying the resulting Fe_3O_4@SiO_2 nanoparticles at room temperature. In Figure 3, it is shown that.

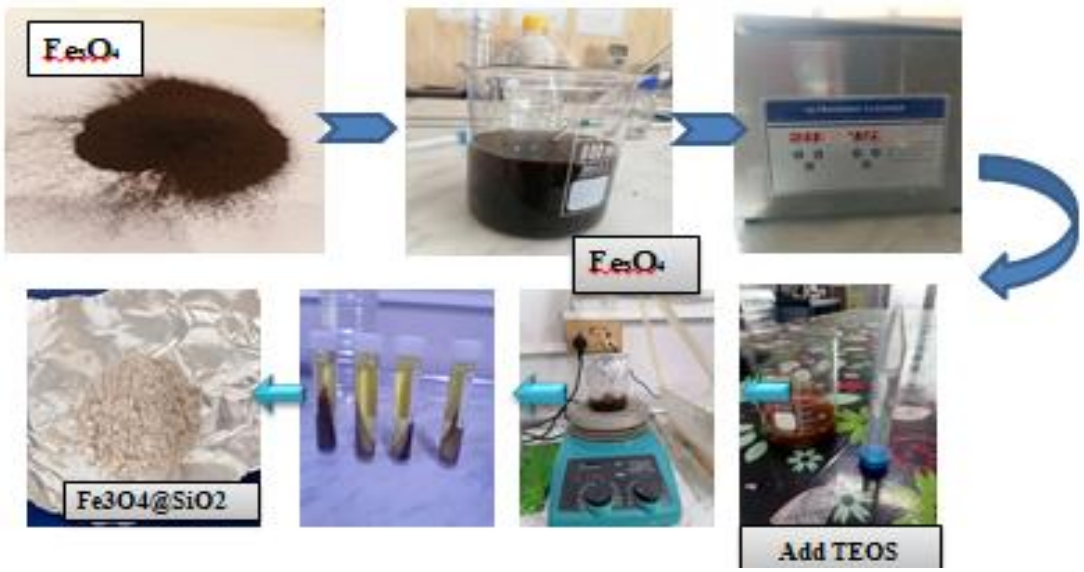

Figure 3. Synthesis of Fe_3O_4@SiO_2 Nanoparticles (MNPs).

2.6. Synthesis of Silver Vanadate $AgVO_3$

Using a simple hydrothermal method, silver vanadate ($AgVO_3$) nanoribbons were produced. The 25 mL water solutions of silver nitrate ($AgNO_3$) and ammonium metavanadate (NH_4VO_3) were mixed continuously for 20 minutes to achieve an equimolar ratio of 0.050 M. A magnetic stirrer was used to homogenize the resultant solution, ensuring the reactants were evenly distributed and allowing nanoribbon structures to form. According to Figure 4, it represents the synthesis of silver vanadate ($AgVO_3$).

Figure 4. Synthesis of Silver Vanadate $AgVO_3$.

2.7. Synthesis of Fe_3O_4@SiO_2@$AgVO_3$ core/shell Magnetic Nanocomposites (MNCs)

The magnetic nanocomposites Fe_3O_4@SiO_2@$AgVO_3$ were synthesized using a co-precipitation technique. To make a uniform suspension, 0.1 g of the synthesized Fe_3O_4@SiO_2 MNCs was mixed with 20 mL of deionized water and then subjected to ultrasonication for 30 minutes. Then, to ensure that the $AgVO_3$ coated the

Fe_3O_4@SiO_2 surface evenly, the suspension was agitated on a magnetic stirrer for 3 hours after the addition of the previously prepared nanoribbons. The 80 mL of the resultant mixture was placed in a Teflon-lined autoclave and heated to 200 °C in an electric oven for 24 hours. As shown in Figure 5, the autoclave was left to cool naturally in the oven for an additional 24 hours after the reaction was complete before being opened. The final Fe_3O_4@SiO_2@$AgVO_3$ magnetic nanocomposites were produced by meticulously collecting the product, magnetically separating it, washing it multiple times with deionized water and ethanol to remove any remaining contaminants, and finally drying it at 60 °C.

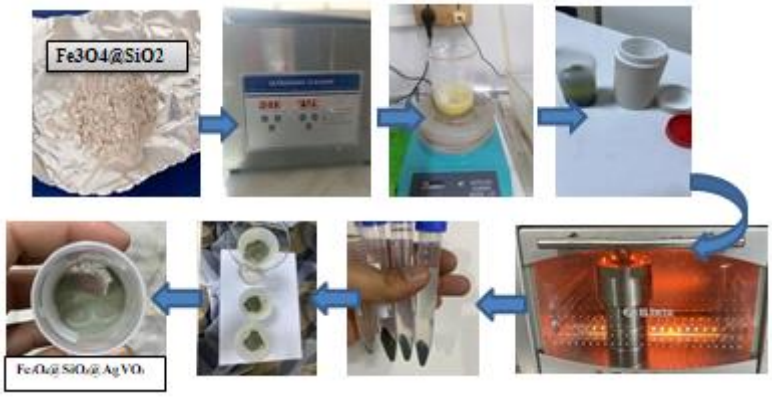

Figure 5. Synthesis of Fe_3O_4@SiO_2@$AgVO_3$ core/shell Magnetic Nanocomposites (MNCs).

2.8. Assembly of Fe_3O_4/SiO_2/$AgVO_3$ Supported Nanocomposite Photocatalysts:

The SiO_2-coated Fe_3O_4 nanoparticles were suspended in 50 mL of deionized water. Then, the previously prepared $AgVO_3$ nanoribbons were added to the suspension. The mixture was agitated on a magnetic stirrer for 3-4 hours to ensure a uniform $AgVO_3$ coating on the Fe_3O_4@SiO_2 surface. After separating the composite product using magnetic decantation, it is washed many times with a mixture of deionized water and ethanol. After that, it is dried at 60°C for 12 hours. As shown in Figure 6.

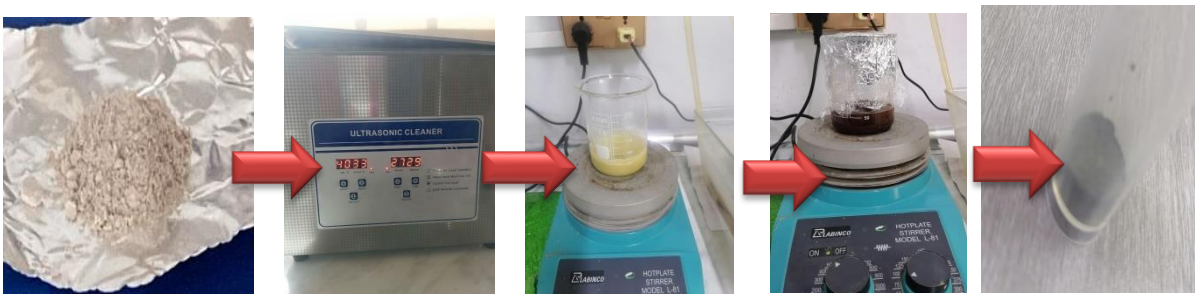

Figure 6. Synthesis of Fe_3O_4/SiO_2/$AgVO_3$ Supported Nanocomposite Photocatalysts.

3. Characterization

3.1. Vibrating sample magnetometer (VSM)

The magnetic properties of the developed materials, as illustrated by the Vibrating Sample Magnetometry hysteresis loops in Figure 7, are invaluable information on the phase structure and the structure of the Fe_3O_4 nanocomposites. Sample (a) of magnetite is the strongest due to the lack of other non-magnetic additives, and its saturation magnetization (M_s) is the largest since at room temperature, the remanence (M 7) and coercivity (H 0) are zero [29], [30]. The behavior is maintained in all the modified samples, even the silica-coated Fe_3O_4 at SiO_2 (b), but a slight reduction in the value of M_m can be observed. This reduction can be mainly attributed to the mass dilution effect of the diamagnetic shell of the SiO_2 or either of the two Fe_3O_4@SiO_2 interfaces, which raises the total mass of the composite without adding to the overall magnetic moment, and the possibility of surface spin disorder at the interface of the two materials [30], [31]. The introduction of the core-shell (c) and the supported (d) versions of the sample with silver vanadate ($AgVO_3$) leads to a further

decrease in the values of saturation magnetization, since now the sample has a larger volume fraction of the non-magnetic catalytic phases [30], [31]. The core-shell structure (c) typically provides a less heterogeneous shielding of the magnetic core than the supported one (d), where the nanoparticles of the magnetic core (i.e., Fe_3O_4) are dispersed in the matrix of $SiO_2/AgVO_3$; however, both are sufficiently magnetically responsive to retrieve them rapidly with the assistance of an external magnetic field [15], [32]. Lastly, the progressive decrease of the Ms of the original Fe_3O_4 to the multi-component system of the $Fe_3O_4/SiO_2/AgVO_3$ system validates the successful integration of the non-magnetic layers without compromising the core super paramagnetic properties of the system required to accomplish an efficient catalytic recycling [33], [34].

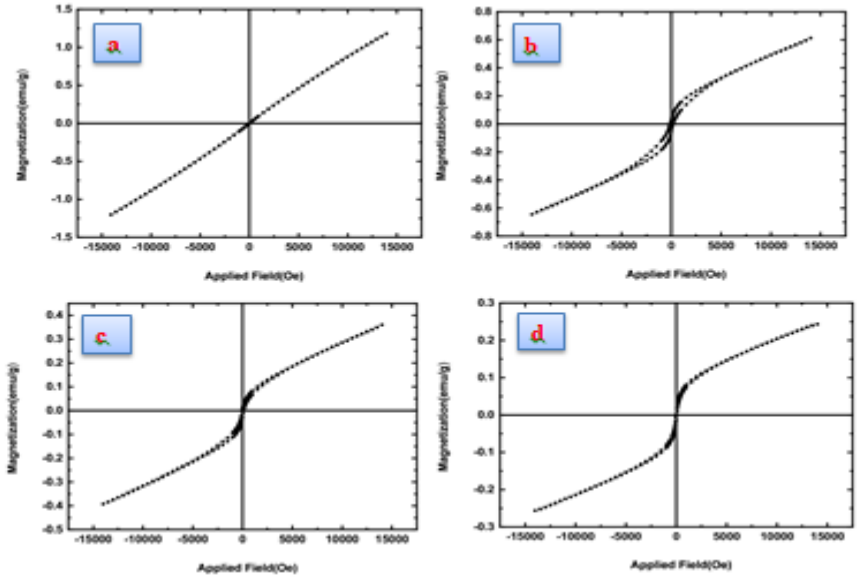

Figure 7. Magnetic hysteresis curves of (a).Fe_3O_4, (b). $Fe_3O_4@SiO_2$, (c).$Fe_3O_4@SiO_2@AgVO_3$ cor&shell, (d). $Fe_3O_4/SiO_2/AgVO_3$ supported.

3.2. Atomic Force Microscope (AFM)

The characterization of the treated materials was done with the help of atomic force microscopy (AFM) as shown in figure 8, 9, and 10 respectively. The AFM technique was used to measure the surface roughness, topography, morphology, and average diameter of the particles in this study. This method was used to study the morphology of the surface of the nanoparticles through AFM, which is an atomic force microscope (AFM). The structure of the green-synthesized Fe_3O_4 is explored by the analysis of the atomic force microscopy showing the apparent morphology of the material is a sphere, with the topography of the material being three-dimensional, demonstrating the effective reduction and stabilization of the magnetite core during the plant-mediated syntheses [13], [30], [33], [5]. The size range of such nanoparticles is usually about 50-60 nm, but there is a certain amount of agglomeration that is observed in the topographical maps due to high surface energy and natural magnetic dipole attractions. With respect to Sample 2 ($Fe_3O_4@SiO_2$), the results of AFM measurements have shown that the height and diameter of the particles have grown at a certain rate that implies the formation of a silica shell protecting the magnetic core and trying to prevent its oxidization and leaching in water [1]. Quantitative measurements of surface roughness on a surface (average roughness, R_a, and root mean square roughness, Rq) and the transition of the raw core and the coated intermediate were measured, and the resultant heterogeneous surface topography is the key to maximizing the active sites used in subsequent loading of $AgVO_3$ and adsorption of methylene blue [2], [3].

Finally, the AFM results confirm the structural integrity and large surface area of the magnetic composite, which consequently guarantees its effectiveness in the removal of dyes and the successful recovery of a solution with the help of an external magnetic field.

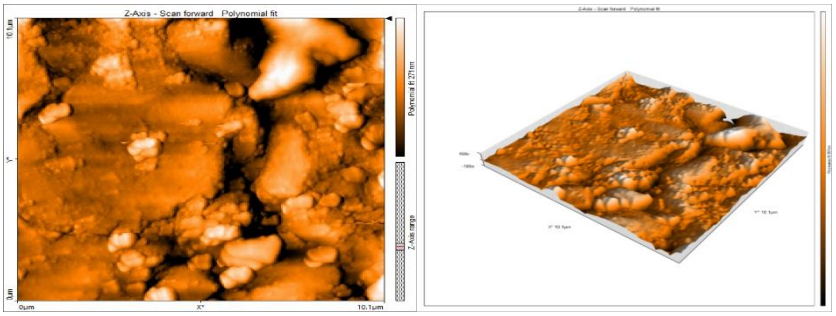

Figure 8. AFM images for nanoparticles; (Left) 2D and (Right) 3D, Fe_3O_4.

The Average (Mean) Diameter of nanoparticles = 58.36nm, Fe_3O_4. The average (Mean) Diameter of nanoparticles = 41.42nm, Fe_3O_4@SiO_2, and the average (Mean) Diameter of nanoparticles = 49.18nm, Fe_3O_4@SiO_2@$AgVO_3$ respectively.

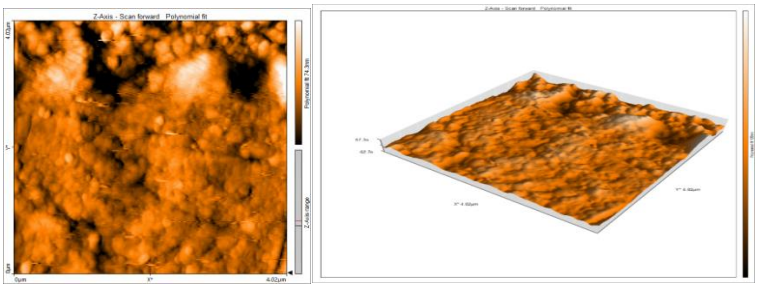

Figure 9. The AFM images for nanoparticles; (Left) 2D and (Right) 3D, Fe_3O_4@SiO_2,

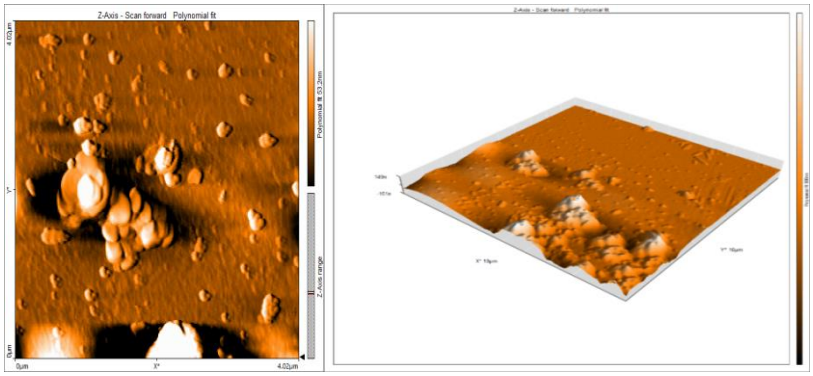

Figure 10. The AFM images for nanoparticles; (Left) 2D and (Right) 3D, Fe_3O_4@SiO_2@$AgVO_3$,

3.3. TEM

The visual information of the transmission electron microscopy (TEM) images provides the in-depth visual information of the morphology of the Fe_3O_4 at SiO_2 at $AgVO_3$ core-shell nanocomposite. The shots unveil the structural aspects of the material at different magnifications, therefore giving it its nanoscale properties as shown in figure 11. The calibrated first left image with a scale bar of 0.8 mm shows a macroscopic image with the elongated or fibrous structural motifs being observed in the composite. The main picture, whose size is 200nm, provides a narrowed outlook, which discloses granular details. Here, the composite has a complicated morphology with a mixture of various-sized particles, thereby confirming the core-shell structure: Fe_3O_4 is the core and SiO_2/$AgVO_3$ is the shell. The most interesting structural details are seen in the rightmost image, multiplied by 100 nm, which provides a clue to the interaction of the core and shell components and the spatial distribution of the layers of silver vanadate and silica. These TEM observations cannot be avoided in understanding the physical properties of the core/shell nanocomposite. The fact that the variation of the particle size and distribution exists suggests that the material can be used as a photocatalyst in a more environmentally related environment. It is also likely that the morphological characteristics determined will

improve the surface area and active sites of the composite, which will lead to its photocatalytic activity in the degradation of synthetic dyestuffs, such as MB.

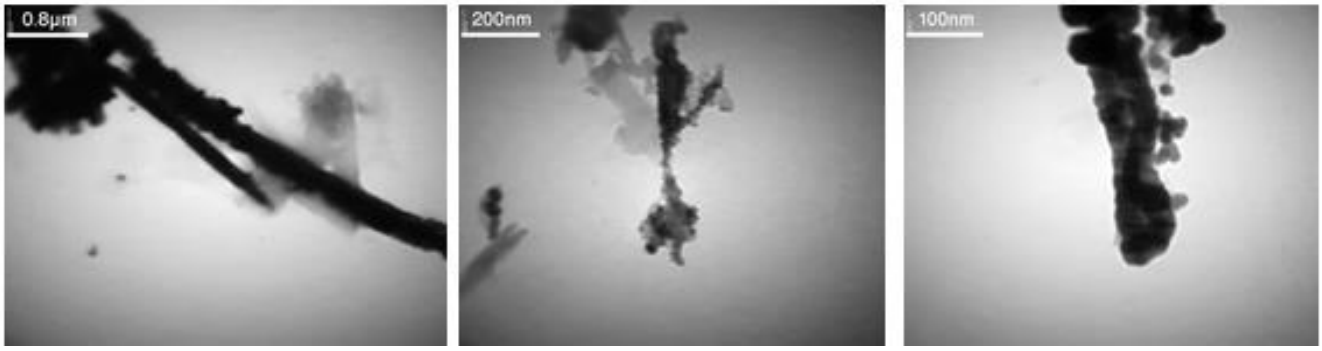

Figure 11. The TEM image for the core/shell nanocomposites

Figure 12 illustrates the morphology of the $Fe_3O_4/SiO_2/AgVO_3$-supported nanocomposite at different magnifications using TEM. The first picture has a scale bar annotated with a 0.4 µm, and the scale bar shows long and fibrous structures in the composite. These morphologies can be aligned with Fe_3O_4 cores with the potential of encasing SiO_2 and $AgVO_3$, therefore a core shell or supported structure. As they appear to be well-oriented, the fibers, to some degree, suggest an ordered or directional morphology, which can favor an increase in the surface area and catalytic activity of the nanocomposite.The other image with the scale bar of 0.8 µm depicts a smaller image with a greater distribution of fibers and particles. The individual particles in this instance are long, thin rods as well as more irregularly shaped particles in addition to $Fe_3O_4/SiO_2/AgVO_3$ nanocomposite; this indicates that the material is a heterogeneous dispersal of the material constituents. This heterogeneity is critical to the photocatalytic works, as it increases the surface area and the active sites that increase the efficiency of degrading dyes such as methylene blue. Overall, the TEM observations show the nanostructure of the $Fe_3O_4/SiO_2/AgVO_3$-supported composite and indicate that the long fibrous nature and the particle size distribution are the factors that render it an efficient photocatalyst. The high-order structure that forms the material in the environmental cleanup processes supports the effective morphology, high surface area, and high concentration of active sites.

Figure 12. The TEM image for supported nanocomposite.

In TEM images of the core/shell nanoparticles, we obtain spherical cores encompassed by thin shell layers. The individual nanoparticles were approximately 20–50 nm, but some aggregates and reasonable rod-like structures are observed in the range up to 500 nm. The small difference in particle sizes is due to (i) the nucleation and growth process involved in shell formation, slightly increasing the dimensions of particles and (ii) aggregation effects regulated by the material of the shell, stabilizing these cores and preventing those from intense clusters. The core/shell architectural design minimizes electron–hole recombination through the shell protective shield (improves photocatalytic performance), while the core absorbs light and generates charge carriers (providing active sites). Proposed Charge Transfer Mechanism: excitation of electrons from valence band of $AgVO_3$ to conduction band of host material yields reactive radicals ($\bullet OH$, $\bullet O_2^-$) that degrade

Methylene Blue (MB) In comparison to previously reported nanocrystals, the core/shell composites found here are smaller and more uniformly coated with shells, which enhances their stability and photocatalytic efficiency.

The TEM images reveal nonbranched rod like structures for supported nanoparticles with lengths of 200–800 nm and diameters ranging from 50 to 150, depending on particle size. The rods look to be well-dispersed and show limited aggregation from the support matrix, while providing additional surface area for MB adsorption. Such structural distribution of the supported nanoparticles promotes electron transport and effective interaction with photocatalytic dye molecules. These findings are in line with earlier reports concerning supported nanorod systems which suggest that well dispersed high aspect ratio structures yield superior photocatalytic activity.

In general, the morphologies of both the core/shell and supported nanoparticles–which were suitable for effective MB degradation with particle size, shell coverage, and support structure as direct factors determining photocatalytic performance.

The TEM images of the Fe_3O_4@SiO_2@$AgVO_3$ core/shell nanoparticles showed the presence of well-defined Fe_3O_4 core and SiO_2 shell with $AgVO_3$ on the surface. The Fe_3O_4 cores' particle size was seen to be in the range of 20–50 nm, and the SiO_2 coating was determined to increase the particle size to be approximately 50–80 nm, depending on the thickness of the coating. This size increase has been observed to correspond with the development of a uniform shell to stabilize the core and to inhibit aggregation. The shell also contributes to increasing the photocatalytic efficiency by promoting charge separation and increasing the surface area to adsorb Methylene Blue.

4. Effect of Experimental Conditions on Photocatalytic Performance

The synthesized Fe_3O_4/SiO_2/$AgVO_3$ nanoparticles were tested with a model dye Methylene Blue (MB) to measure photocatalytic performance. The degradation efficiency was explored under various experimental conditions such as pH of the solution and addition of H_2O_2. The morphological and structural properties of the nanoparticles, derived through TEM, AFM and other techniques, were analysed to determine how these properties effected the photocatalytic activity. The role of particle architecture on improving charge separation, adsorption capacity and the overall degradation efficiency was tested for both core/shell and supported nanostructures. The detailed results of these experiments, together with a discussion in comparison with the previous literature, are presented in the following sections.

The photocatalytic activity of a visible-light reactor was studied on various samples such as Fe_3O_4, Fe_3O_4@ SiO_2, Fe_3O_4@SiO_2@$AgVO_3$, and Fe_3O_4/SiO_2/Ag_2VO_3 supported. Methylene Blue ($C_{16}H_{18}ClN_3S \bullet 3H_2O$) was used in a photocatalytic degradation experiment that was carried out for the evaluation. The dye was analyzed by a UV spectrophotometer (UV-1200 Spectrophotometer, China). The photocatalytic reactor was a 100 mL glass beaker that was irradiated by a visible light source. Three 50-watt LED lights were used in the visible lighting system. In the experiment, a fan was fitted inside the reactor that pushed the air out of the reactor as depicted in Figure 6. This additive can be used to enhance the rate of photocatalytic degradation of the dye by enhancing oxygen diffusion in the solution and, consequently, the reaction rate by blowing down the amount of air introduced into the reactor. A mixer was used to keep the photocatalyst suspension in the reactor, making sure that all of the components blended evenly. The photocatalytic mechanism was based on the mixer to keep the photocatalysts in suspension in the MB dye solution. The first experiment used a 100 mL sample, of which a 40 ppm concentration of MB dye solution was prepared. Several synthetic photocatalysts, such as Fe_3O_4, Fe_3O_4/SiO_2, Fe_3O_4@SiO_2@$AgVO_3$, Fe_3O_4/SiO_2/$AgVO_3$ supported, were added to the MB dye solution at a dosage of 1 g/L (100 mg) of catalysts. In order to achieve absorption-desorption equilibrium, the whole solution was swirled 60 minutes in the dark. Photocatalysis of the MB dye was done to break up after an additional 120 minutes of exposure to the visible light source. A UV spectrophotometer was employed at 665 nm to measure the residual MB concentration; 3 mL of the deteriorated sample were collected after every 10 minutes [30]. The diagrams indicate the photocatalytic performance in this experiment, without the participation of additional chemicals like hydrogen peroxide (H_2O_2). The degradation performance (DP) of each of the photocatalysts has been obtained by using the following equation (Eq. 1) [18].

$$DP\ (\%) = (C_0 - C_t)/C_0 \times 100 \quad (1)$$

Where C_0 is the initial concentration and C_t is the final concentration of the MB solution after the photocatalysis process. The figures 13 and 14 represent the diagrammatic representation of the batch reactor used for the degradation of MB dye.

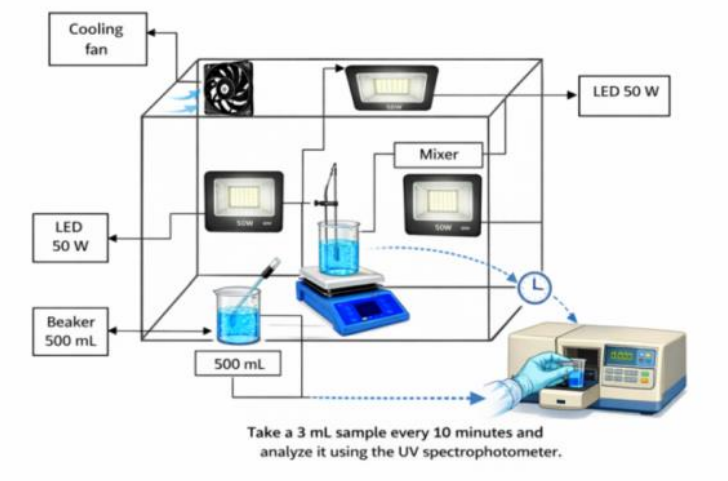

Figure 13. Diagrammatic representation of the photocatalytic reactor system for MB dyes degradation when exposed to visible light.

Figure 14. The batch reactor of the photocatalytic system to remove MB from synthetic wastewater using various types of catalysts.

The figure 15 represents the de-coloration of the methylene blue that is expressed in time when various catalysts are added under the given experimental conditions, i.e., in the absence of hydrogen peroxide and at a pH of 5. The data sets were associated with four composite materials that had three varying quantities of Fe_3O_4 at the core and four varying quantities of SiO_2 at the core and $AgVO_3$ (core-shell) or on the support ($Fe_3O_4/SiO_2/AgVO_3$); the various removal efficiencies were reported at the end of the experimental period.
The least removal efficiency of Fe_3O_4 is 33%, and this implies that in the specified conditions, the specified substance is relative to degrading methylene blue. Gradually increasing the amount of silica (SiO_2) in the Fe_3O_4 composition increases the removal efficiency up to 62 000, indicating that the addition of silica (SiO_2) to the Fe_3O_4 composition improves the catalytic activity of the latter. The core-shell composite $Fe_3O_4@SiO_2@AgVO_3$ is even more efficient, at 70, and the presence of the silver vanadate ($AgVO_3$) compound and the core-shell structure itself has a significant contribution to the photocatalytic activity, which renders the material more efficient for dye degradation. The $Fe_3O_4/SiO_2/AgVO_3$ supported composite is the most efficient with a removal efficiency of 79%, meaning that the mixture of Fe_3O_4, SiO_2, and $AgVO_3$ in supported form offers the most efficient dye removal. Such high performance is likely to be attributed to a more uniform distribution of active sites and the ability to catalyze photocatalytic behavior given the presence of $AgVO_3$ and the architecture in which it is anchored. Lastly, the figure demonstrates that the photocatalytic activity of the degradation of methylene blue is increased greatly by the incorporation of SiO_2 and $AgVO_3$ and that the composite of the $Fe_3O_4/SiO_2/AgVO_3$ is the most efficient under the specified conditions of the experiment.

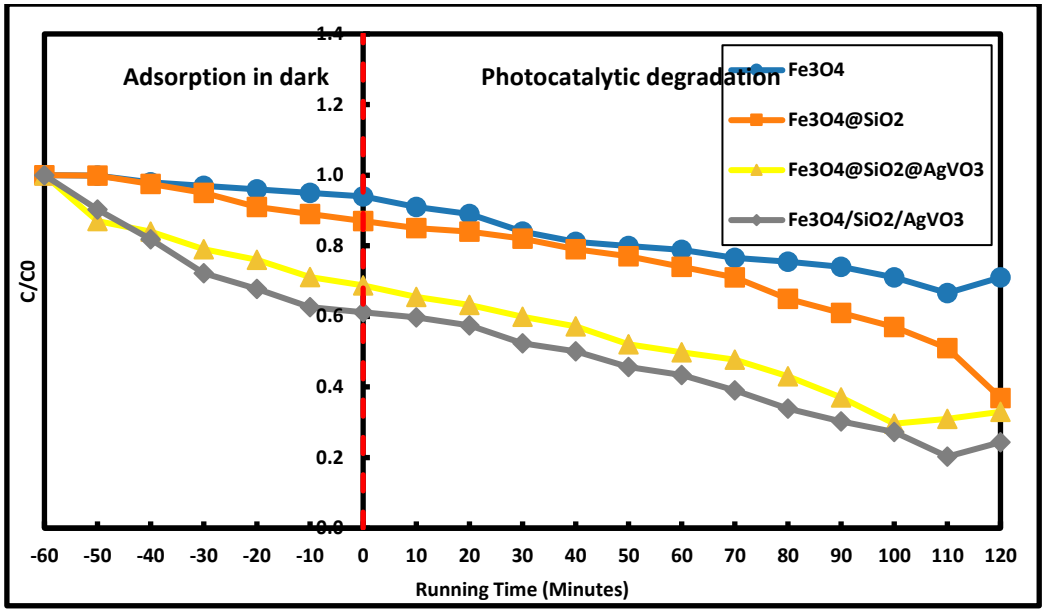

Figure 15. Removal Efficiency of Methylene Blue Over Time Using Catalysts without H_2O_2.and pH=5: (a).Fe_3O_4 33%, (b). Fe_3O_4@SiO_2 62%, (c).Fe_3O_4@SiO_2@$AgVO_3$ cor&shell 70% , (d). Fe_3O_4/SiO_2/$AgVO_3$ supported 79%.

Figure 15 demonstrates the performance of each of the composites in two different periods: the adsorption period that is conducted in the dark and the photocatalytic degradation period that is conducted in the presence of light. One of the steps is a dark adsorption phase, in which all the composites show a decrease in the C/C_0 ratio, hence indicating the adsorption of methylene blue on the photocatalytic surfaces. Out of the investigated composites, Fe_3O_4@SiO_2@$AgVO_3$ shows the strongest adsorption, as it shows the highest initial decrease in the C/C_0 ratio, and subsequent to it is Fe_3O_4/SiO_2/$AgVO_3$. On the other hand, the adsorption capacity of Fe_3O_4 and Fe_3O_4 at SiO_2 is relatively lower in Fe_3O_4. When it is illuminated, the photocatalytic degradation phase starts. The maximum photocatalytic efficiency is Fe_3O_4/SiO_2/$AgVO_3$, with the lowest C/C_0 ratio at the end of the experiment, and the final efficiency is 36.5. The Fe_3O_4 @ SiO_2 and Fe_3O_4 have relatively low degradation efficiencies, and the final efficiencies of the two are 22.1% and 49.5%, respectively.

The results clearly show that the addition of SiO_2 and $AgVO_3$ increases the photocatalytic activity of Fe_3O_4 and that the Fe_3O_4@SiO_2@$AgVO_3$ hybrid has the best performance in the degradation of methylene blue. The paper also unveils the importance of composite architecture and surface modification in making the photocatalytic ability of materials used in cleaning the environment. Figure 16 shows the time dependence of the removal efficiency of MB dye with catalysts in the absence of H_2O_2 and pH=7: (a) Fe_3O_4 61%, (b). Fe_3O_4@SiO_2 77% (c); Fe_3O_4@SiO_2@$AgVO_3$ core&shell 83% (d). Fe_3O_4/SiO_2/$AgVO_3$ supported 89%. In figure 16, it explains the relationship between time and removal efficiency (percent) of both the dark and light degradation of core/shell and supported nanocomposite. The methylene blue degradation in the synthesized magnetic composites is a kinetic reaction in two steps and starts with an initial step of dark adsorption-desorption equilibrium and is followed by a second step of degradation that is light. In this case, the poorest performance is noted under the green bar of the nanoparticles having the final C/C_0 ratio of 0.505, which can be used to rationalize the lower intrinsic photocatalytic activity of magnetite. On the other hand, the removal of dyes is significantly increased with the addition of a silica shell in the Fe_3O_4@SiO_2 composite (C/C_O = 0.221) and the inclusion of silver vanadate in the Fe_3O_4/SiO_2/$AgVO_3$ (C/C_O = 0.270) and Fe_3O_4@SiO_2/$AgVO_3$ (C/Co = 0.365) systems due to the provision. The additional layer of SiO_2 works as a protective layer, which is important in the elimination of the photodissolution of the magnetic core, and concurrently, it allows the uniform distribution of the $AgVO_3$ catalyst on the surface. Lastly, the superparamagnetic properties also contribute to the high efficiency of the ternary composite by being able to regenerate it in the aqueous media using an external magnetic field within the shortest time possible, a property that is also important and enables the practical reuse of the catalyst in environmental cleaning [31].

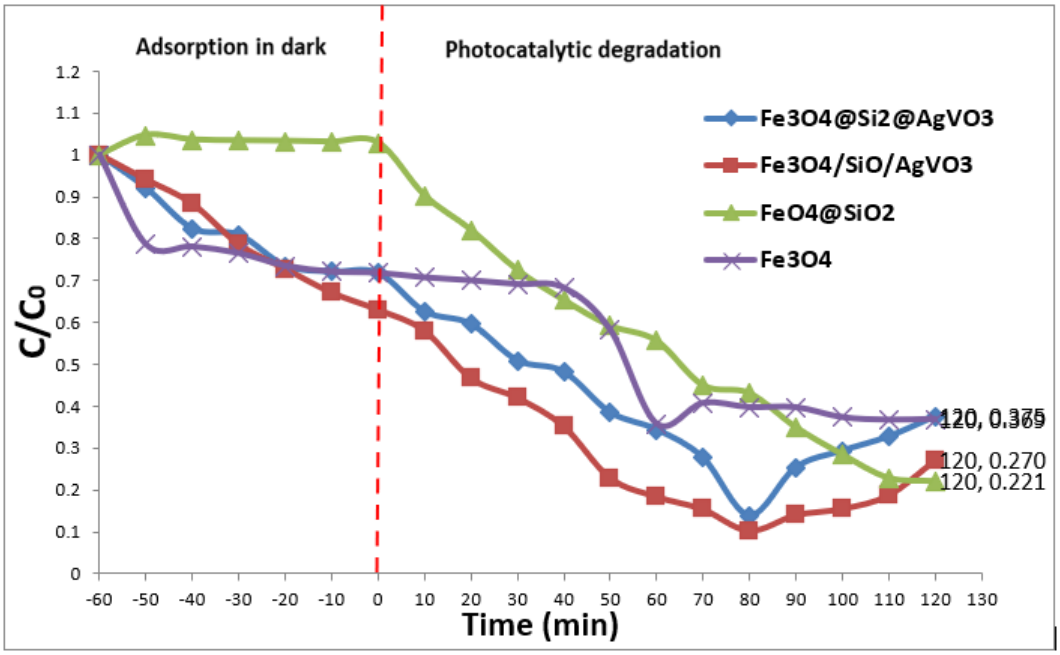

Fi=gure 16. Comparison of Photocatalytic Degradation Efficiency of Various Photocatalysts without H_2O_2.and pH=7: (a).Fe_3O_4 61%, (b). Fe_3O_4@SiO_2 77%, (c).Fe_3O_4@SiO_2@$AgVO_3$ cor&shell 83%, (d). Fe_3O_4/SiO_2/$AgVO_3$ supported 89%.

Figure 17 shows the change of Methylene Blue removal efficiency with time in relation to time and two different catalytic systems: core-shell catalysts (supported assembly of Fe_3O_4 siloxane-coated, siloxane-coated, and $AgVO_3$) and single-shell catalysts (Methylene Blue removal) depending on Fe_3O_4. The two systems are effective in the presence of hydrogen peroxide (H_2O_2) and neutral pH (pH = 7). The figure 17 offers a dark-phase adsorption step and light-phase photocatalytic degradation step and compares the catalytic activity of the two continuous operating processes. As the time becomes zero, a red dashed line shows the boundaries of the steps in respect to time. Sequential decrease of the ratio of concentration of the dye (C/C_0) of the two catalysts in the process of adsorption indicates the adsorption of methylene blue on the surface of the catalyst. The core-shell catalyst Fe_3O_4/SiO_2/$AgVO_3$ is in the intermediate adsorption capacity with the decrease in C /Co ratio. Conversely, the core-shell catalyst exhibits a lower rate of adsorption compared to the heavily adsorbed catalyst Fe_3O_4/SiO_2/$AgVO_3$ and this indicates that the catalyst could have a higher adsorption capacity. On being subjected to light, the photocatalytic breakdown process initiates and the C/C_0 ratio varies greatly in both composites, which means that the methylene blue has been successfully decolorized. The core-shell catalyst Fe_3O_4@SiO_2@$AgVO_3$ with a final efficiency of 89% was the most degraded, then the supported catalyst Fe_3O_4/SiO_2/$AgVO_3$ with a final efficiency of 91%. These results reflect the overall dye removal performance of the supported design as compared to that of core-shell arrangement, but in an insignificant manner. These findings showed that using either composite in the presence of H_2O_2 (120 mM) at neutral pH enhanced catalytic activity, but the supported catalyst was slightly better, according to these findings. This behavior change can be attributed to the composition and structure of the two catalysts which is different. Specifically, the supported design enables the separation of charge carriers and production of photogenerated reactive species to be more efficient because of the limited contact of the interfaces. The structural organization is essential to enhance photocatalytic processes of environmental cleaning and to optimize the degrading efficacy of MB. The concentration of the hydrogen peroxide is 120 mM was added in the experimental study.

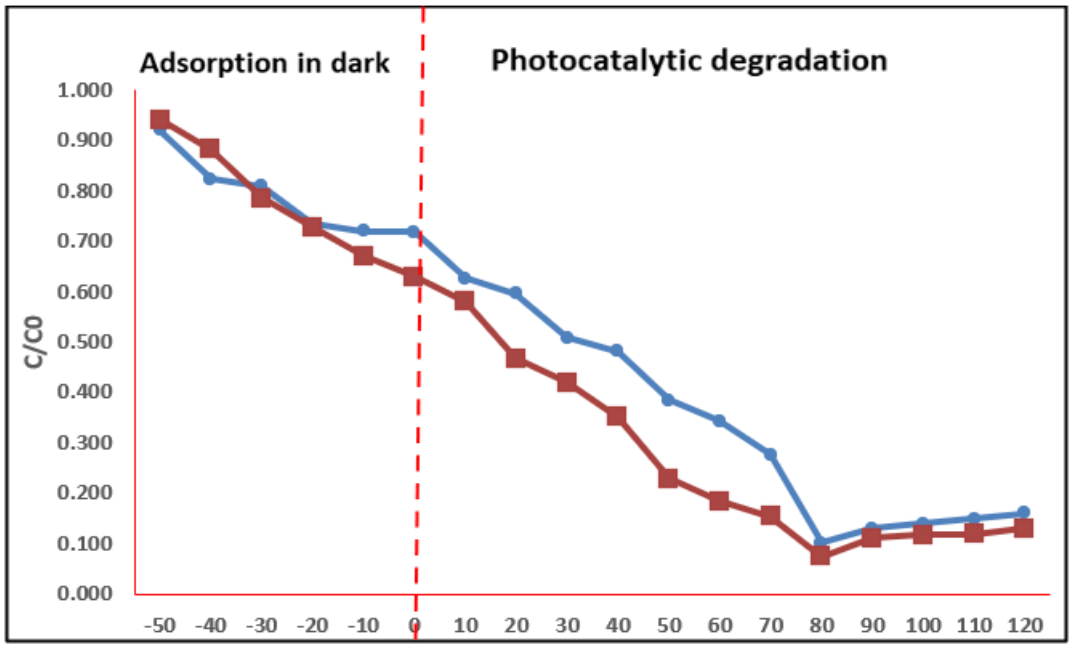

Figure 17. Removal Efficiency of Methylene Blue Over Time Using Catalysts with H_2O_2 (120 mM) and pH=7: (a) Fe_3O_4@SiO_2@$AgVO_3$ cor&shell 89% (b). Fe_3O_4/SiO_2/$AgVO_3$ supported 91%

In summary, the work offers a general assessment of photocatalytic degradation of methylene blue by disparate composite systems, i.e., Fe_3O_4, Fe_3O_4@SiO_2, Fe_3O_4@SiO_2@$AgVO_3$ (core-shell) and Fe_3O_4/SiO_2/$AgVO_3$ (supported) under numerous experimental The data was classified into three analytical sections with the following conditions: pH=5, pH=7 and the presence of H_2O_2 at the neutral pH. Within the primary segment (the aqueous medium was acidified to pH 5) the composites performed with different efficacies in rectifying methylene blue. The efficiency of the apex removal of the Fe 3 O 4 core/shell assembly at the Fe_3O_4 core/ shell assembly was 70, and then the Fe_3O_4/SiO_2/$AgVO_3$ composite at the supported level exhibited an 79 yield. The unmodified Fe_3O_4 at SiO_2 and the non-modified Fe3O4 counterparts had rather low performance, with the removal efficiencies of 62% and 33%, respectively. These experiments underscore the auxiliary power of surface engineering, notably silica and silver vanadate shelling, to enhance the kinetic of the photocatalytic degradation with the configuration on top having the highest performance [13], [14].

The overall degradation rate increased in all the composite types in the second part which operated in neutral conditions (pH=7). The construct that showed the highest efficiency was the one containing the supported Fe_3O_4/SiO_2/$AgVO_3$, with the construct giving a result of 91%, and the core-shell Fe_3O_4@SiO_2@$AgVO_3$ construct a result of 89. The Fe_3O_4 at SiO_2 assembly had an intermediate performance at 77.9 % and the unmodified Fe_3O_4 had the lowest performance with a slight difference at 49.5 %. This trend emphasizes the reality that the state of neutral pH also leads to photocatalytic activity especially with silica-silver vanadate modifier composites. This resulted in a great improvement of photocatalytic degradation in the terminal segment where hydrogen peroxide was introduced and the pH maintained at seven. The highest efficiency of 91% was once again achieved with the supported Fe_3O_4/SiO_2/$AgVO_3$, and secondly, the 89% efficiency of the core/shell Fe_3O_4 is that of the core/shell Fe_3O_4@SiO_2@$AgVO_3$. The Fe_3O_4 at SiO_2 composite showed the highest percentage of 79% to be made and the lowest percentage of 63.5 % was recorded in the Fe_3O_4 at SiO_2 (baseline). This addition of H_2O_2 is therefore favored to enhance the overall degrading capacity by enhancing the reactive oxygen species which in turn promotes the photocatalytic reaction [32], [33].

Combined, the findings are effective evidence that addition of silica and silver vanadate substantially enhances the rate at which methylene blue breaks down in varying pH regimes in photocatalytic process. The latter trend is expected to provide better performance of the variant of Fe_3O_4/SiO_2/$AgVO_3$ that is supported, followed by the core-shell Fe_3O_4@SiO_2@$AgVO_3$. The added hydrogen peroxide leads to further enhancement of performance, which indicates the possibilities of the systems in terms of effective and sustainable

wastewater treatment. The study identifies catalyst compositional refinement and environmental modulation as the most important factors towards high photocatalytic degradation efficiencies [31].

Photocatalytic experiments of synthesized nanoparticles were conducted by evaluating the variation of Methylene Blue (MB) degradation under visible light. The degradation efficiency was 91% and 89%, respectively from supported and core/shell nanoparticles in the first 120 minutes. These results mean that the supported structure offers more efficient charge separation and interaction with MB molecules than those of supported system. This performance is in agreement with the previous literature since metallic core/shell architectures usually demonstrate enhanced efficiencies. The mechanisms of higher efficiency are mainly attributed to electron–hole separation and increased surface active sites [32], [33], [34].

5. Comparative studies

Ideally, photosynthetic catalysts that are magnetically accessible should be used, since this will enable the catalyst to be easily and completely isolated out of the catalyst environment. The most common method of recovery and reuse of photocatalysts is centrifugation and flotation; ferrites can potentially provide a significant enhancement [30]. Quantum-confined nano-ferrites are the most promising materials that can be used to generate highly efficient photocatalysts because they have high surface area compared to their volume. Salman [6] reported that the synthesized activated carbon and NiO nanoparticles were examined using Brunauer-Emmett-Teller, scanning electron microscopy with energy-dispersive X-Ray spectroscopy (EDX), Response Surface Methodology (RSM) was used in Design-Expert (13 Stat-Ease) to investigate the impact of different factors such as malachite green concentration, pH, contact time, and dosages of NiO, AC, and NiO/AC. It was found that the maximum removal efficiency of malachite green dye occurred when the initial concentration was 150mg/L, pH was 4, contact time was 120minutes and adsorbent dosage was 0.25 g/L giving a 97.92%, 98.89% and 99.98 % removal efficiency. The Langmuir, Freundlich, and pseudo-first-order and pseudo-second-order kinetic models were used to analyze the equilibrium adsorption data. The findings showed that the Freundlich isotherm and pseudo-second-order kinetic equation were the most efficient to describe the data of the adsorption equilibrium [6].

Table 4. The different comparative studies are discussed in the following table.

Nanomaterial	**Dosage**	**Pollutant**	**Light Source**	**Reaction Time**	**Efficiency**	**Reference**
ZnO nanoparticles	0.5 g/L (tea extract)	Clomazone, Tembotrione, Ciprofloxacin, Zearalenone	Simulated sunlight	Varied (optimum)	95–98%	[4]
Co-doped CuO NPs	1.0 g/L	Methylene Blue (MB)	UV-Vis light	100 min	88%	[15]
Ag-CuO NPs	0.5 g/L (Moringa)	Methylene Blue (MB)	Visible light	80 min	95%	[11]
Ag_2O@CuO	0.2 g/L	Rhodamine B (RhB)	UV light	90 min	90–98%	[16]
TiO_2-CeO_2	1.0 g/L TiO_2	Methylene Blue (MB)	Simulated sunlight	150 min	95%	[8]
$Fe_3O_4/SiO_2/AgVO_3$	0.1 g/L	Methylene Blue (MB)	Visible light	140 min	90%	This study

6. Conclusions

A green route synthesis was effective in this paper to produce magnetic nanocomposites of Fe_3O_4 coated with SiO_2 and $AgVO_3$ to obtain highly efficient, magnetically recoverable materials in aqueous contaminants removal. The synthesis was environmentally friendly with minimal utilization of toxic reagents, which are in line with sustainable methods of nanomaterials synthesis and environmental remediation efforts. Two different methods were synthesized in two structure which are core/shell and supported structures. The

synthesized $Fe_3O_4/SiO_2/AgVO_3$ nanocomposites demonstrated high removability, of about 91% with the supported structure and about 89% with the core-shell construction **$Fe_3O_4@SiO_2@AgVO_3$**. VSM characterization ensured the strong magnetic properties, enabling the rapid magnetic separation and recovery, and AFM and TEM analyses highlighted uniform morphology and formation of core-shell architecture, confirming structural stability of the synthesized nanomaterials. The use of the SiO_2 interlayer was an effective way to stop agglomeration and increase the dispersion of the surface active sites, reminiscent of the earlier reports on the core shell magnetic composites, where silica shells were used to enhance stability and usefulness of the material in environmental applications. Other studies have shown that the magnetic core-shell structures with functional shells can considerably improve the photocatalytic or adsorption activity and ease the magnetic recovery of aqueous systems. Altogether, the $Fe_3O_4/SiO_2/AgVO_3$ nanocomposites green-synthesized have good chances of successful efficacy, durability, and recyclability which help to justify their perspectives as sustainable candidates to the progressive wastewater treatment systems. Future studies can extend to explore long-term recyclability and performance on actual wastewater matrices.

Declaration of Competing Interest

The authors declare that there are no conflicts of interest regarding the publication of this manuscript.

Funding Information

No funding was received from any financial organization to conduct this research

Author Contributions

All authors proposed the research problem. In addition to author Dr. Nuralhuda Aladdin Jasim collected recent articles and organized them in simple shapes. Authors **Alaa Kharbat Shadhar** verified the recommendation in the proposed work. All the authors discussed the results and the final version of this paper.

Acknowledgments

The authors express their gratitude to Wasit University/ College of Engineering/Civil Engineering department in Alkut-Wasit-Iraq for supporting this study. In addition, many thank to Dr. Nuralhuda Aladdin Jasim and Dr. Alaa Kharbat Shadhar for their advice for the academic writing of this paper.

References

[1]. A. M. Abu-Dief, W. H. Alsaedi, and M. M. J. Zikry, "A collective study on the fabrication of nano-materials for water treatment," *J. of U. A.-Q. U. f. A. S.*, pp. 1-23, 2025.

[2]. A. Al Miad, S. P. Saikat, M. K. Alam, M. S. Hossain, N. M. Bahadur, and S. Ahmed, "Metal oxide-based photocatalysts for the efficient degradation of organic pollutants for a sustainable environment: a review," *Nat. Agri.*, vol. 6, no. 19, pp. 4781-4803, 2024.

[3]. N. Ali, A. Zada, M. Zahid, A. Ismail, M. Rafiq, A. Riaz, and A. Khan, "Enhanced photodegradation of methylene blue with alkaline and transition-metal ferrite nanophotocatalysts under direct sun light irradiation," *J. of the Chem. C. S.*, vol. 66, no. 4, pp. 402-408, 2019.

[4]. S. Bognár, D. Jovanović, V. Despotović, S. Jakšić, S. Panić, M. Milanović, and D. Šojić Merkulov, "Advanced photocatalytic degradation of organic pollutants using green tea-based ZnO nanomaterials under simulated solar irradiation in Agri-Food wastewater," *J. of F. Chem.*, vol. 14, no. 4, p. 622, 2025.

[5]. P. Chinnakoti, A. D. Kurdekar, K. M. Rao, and V. Kamisetti, "A review of the emerging role of engineered nanomaterials as nanoadsorbents in enhanced drinking water defluoridation," *Desal. Eng.*, vol. 3, no. 1, p. 151, 2025.

[6]. R. M. Hadi, S. D. Salman, "Green synthesis of NiO nanoparticles with activated carbon from Ficus carica leaf and extract for malachite green removal," *Int. J. of Chem. Eng., P.* vol. 26, no. 4, pp. 133-150, 2025.

[7]. M. A. Hassaan, M. A. El-Nemr, M. R. Elkatory, S. Ragab, V.-C. Niculescu, and A. El Nemr, "Principles of photocatalysts and their different applications: a review," *Trends in Chem. Chem.*, vol. 381, no. 6, p. 31, 2023.

[8]. D. Q. Ho, V. D. Lai, Q. A. Nguyen, D. D. Nguyen, and D. D. La, "Green Synthesis of TiO2-CeO2 Nanocomposites Using Plant Extracts for Efficient Organic Dye Photodegradation," *Chem. C.*, vol. 15, no. 6, p. 583, 2025.

[9]. N. A. Jasim, S. E. Ebrahim, and S. H. Ammar, "Photocatalytic degradation of Rhodamine B using CoxZn1-xFe2O4 nanocomposite under visible light irradiation: synthesis, characterization and its application," *J. Appl. Eng. J.*, vol. 82, pp. 557-576, 2023.

[10]. N. A. Jasim, S. E. Ebrahim, and S. H. Ammar, "Visible light-boosted photodegradation activity of Ag–AgVO3/Zn0.5Mn0.5Fe2O4 supported heterojunctions for effective degradation of organic contaminants," *J. Environ. Eng.*, vol. 14, no. 1, p. 20220585, 2024.

[11]. N. Zulfiqar, F. Inam, I. Khudayberganov, and S. Kurbanova, "Sustainable synthesis and photocatalytic insights into Ag-doped copper oxide nanoparticles: a comparative study," *Sustain. Res.*, 2026.

[12]. D. M. Salih and O. H. Yousif, "The Method of on in the Qur'an (A Semantic Study from Interpretation and Language Scholars' Point of View)," *KnE Social Sciences*, vol. 8, no. 6, pp. 216-228, 2023.

[13]. M. Munasir, L. Rohmawati, N. Faaizatunnisa, et al., "The effect of silica mass ratio on pore structure and magnetic characteristics of core-shell nanoparticles," *Journal of Metals, Materials and Minerals*, vol. 34, no. 1, Art. no. 1832, 2024.

[14]. H. Kosslick, Y. Wang, M. F. Ibad, et al., "High-Performance Room-Light-Driven Core/Shell Photocatalyst Prepared by Mechanochemical Method," *Catalysts*, vol. 11, no. 11, Art. no. 1358, 2021.

[15]. D. Masekela, L. K. Kganyakgo, K. D. Modibane, T. L. Yusuf, S. A. Balogun, W. M. Seleka, and E. Makhado, "Green synthesis and enhanced photocatalytic performance of Co-Doped CuO nanoparticles for efficient degradation of synthetic dyes and water splitting," Rev. Chem. Chem., vol. 13, p. 101971, 2025.

[16]. D. M. Mohsen, S. M. Al-Jubouri, S. J. Al-Batty, "Photocatalytic degradation of a cationic dye using Ag2O@ CuO nanoellipsoidal photocatalyst under ultraviolet irradiation," Int. J. Chem. Eng., P., vol. 26, no. 4, pp. 27-40, 2025.

[17]. E. Shargh, H. S. Kalal, Z. Shiri-Yekta, et al., "Isothermal, Kinetic, and Thermodynamic Studies on the Adsorption of Molybdenum by a Nanostructured Magnetic Material," 2020.

[18]. U. Z. Ismaile, K. Bahrami, and M. Khodamorady, " as A Novel Recyclable Heterogeneous Catalyst with Core-Shell Structure for Oxidation of Sulfides," 2023.

[19]. H. Li, H. Jin, R. Li, et al., "Magnetic study on adsorption of methyl orange on nanoparticles," 2024.

[20]. U. Z. I. Al-Zubaidi, K. Bahrami, and M. Khodamorady, " as a novel recyclable heterogeneous catalyst with core–shell structure for oxidation of sulfides," *Scientific Reports*, vol. 14, Art. no. 8175, 2024.

[21]. K. Polat and M. Yurdakoç, "Removal of Malachite Green from Waste Waters by Bentonite Based Photocatalyst Technology," *JOTCSA*, vol. 6, no. 2, pp. 261-270, 2019.

[22]. Z. Duriagina, R. Holyaka, T. Tepla, et al., "Identification of Nanoparticles Biomedical Purpose by Magnetometric Methods," 2018.

[23]. J. A. Fuentes-García, A. Cano, A. Guillén-Cervantes, et al., "Magnetic domain interactions of nanoparticles embedded in a matrix," 2018.

[24]. R. Ramadan, "Enhancement the physical properties of nanocomposite," 2024.

[25]. H. Kosslick, Y. Wang, M. F. Ibad, et al., "High-Performance Room-Light-Driven Core/Shell Photocatalyst Prepared by Mechanochemical Method," 2021.

[26]. C. Fu, X. Liu, Y. Wang, et al., "Preparation and characterization of magnetic visible light photocatalyst for water treatment," 2019.

[27]. A. A. S. Al-Makhathi, H. Khan, S. Malik, et al., "Ternary magnetic silica–graphene oxide composite for remediation of textile dyes from aqueous environment and real samples," 2023.

[28]. Y. Ramanda, N. Nuryono, and E. S. Kunarti, "Synthesis and Application of Nanocomposite as Photocatalyst in Indirect Reduction to Produce Methanol," 2019.

[29]. N. Jasim, Sh. Ebrahim, and S. Ammar, "A comprehensive review on photocatalytic degradation of organic pollutants and microbial inactivation using Ag/AgVO3 with metal ferrites based on magnetic nanocomposites," Cogent Engineering, vol. 10, no. 1, p. 2228069, 2023, doi: 10.1080/23311916.2023.2228069.

[30]. N. Jasim, Sh. Ebrahim, and S. Ammar, "Fabrication of ZnxMn1-xFe2O4 metal ferrites for boosted photocatalytic degradation of Rhodamine-B dye," Results in Optics, vol. 13, p. 100508, 2023, doi: 10.1016/j.rio.2023.100508.

[31]. N. Jasim, Sh. Ebrahim, and S. Ammar, "Photocatalytic degradation of Rhodamine B using CoxZn1-xFe2O4 nanocomposite under visible light irradiation: Synthesis, characterization and its application," Alexandria Engineering Journal, vol. 82, pp. 557-576, 2023, doi: 10.1016/j.aej.2023.09.081.

[32]. N. Jasim, S. Ammar, and Sh. Ebrahim, "Assembling ZnMnFe2O4@Ag-AgVO3 nanostructure heterojunctions for photocatalytically degrading RhB and Pseudomonas aeruginosa bacteria under visible irradiation," Journal of Photochemistry and Photobiology A: Chemistry, vol. 449, p. 115380, 2023, doi: 10.1016/j.jphotochem.2023.115380.

[33]. N. Jasim, Sh. Ebrahim, and S. Ammar, "Visible light-boosted photodegradation activity of Ag–AgVO3/Zn0.5Mn0.5Fe2O4 supported heterojunctions for effective degradation of organic contaminants," Open Engineering, vol. 14, no. 1, p. 20220585, 2024, doi: 10.1515/eng-2022-0585.

[34]. N. A. Jasim, S. E. Ebrahim, and S. H. Ammar, "Photocatalytic degradation of rhodamine B utilizing core/shell structures ($Zn_{0.3}Mn_{0.7}Fe_2O_4$@$AgVO_3$) under the irradiation of visible light: Synthesis, characterization, and its application," AIP Conference Proceedings, vol. 3219, no. 1, p. 020062, 2024, doi: 10.1063/5.0237320.